RSC Advances

PAPER

View Article Online
View Journal | View Issue

Cite this: *RSC Adv.*, 2017, **7**, 23607

Shape-oriented photodynamic therapy of cuprous oxide (Cu_2O) nanocrystals for cancer treatment

Mukesh Lavkush Bhaisare,†[a] M. Shahnawaz Khan,†[ad] Sunil Pandey,†[a] Gangaraju Gedda[d] and Hui-Fen Wu *[abcd]

Received 27th December 2016
Accepted 18th March 2017

DOI: 10.1039/c6ra28705k

rsc.li/rsc-advances

We report a novel method used for the synthesis of cuprous oxide nanocrystals at room temperature by varying the concentration of the reducing agent and probed their photodynamic activity on HeLa cells. Three different shapes of cuprous oxide nanocrystals (NCs) were synthesized, including cubic, hexagonal and octahedral forms, and investigated for their photodynamic properties. Cuprous oxide generated reactive oxygen species (ROS) after irradiation with a green laser ($\lambda = 532$ nm). TEM, XRD, EDX, and FTIR were applied to characterize their shape factors and optical properties. Cubic, hexagonal and octahedral shapes of cuprous oxide nanocrystals were used for photodynamic therapy *via* incubation with HeLa cells and irradiation with a green laser. The octahedral NCs exhibit the highest photodynamic activity for killing HeLa cells, as evaluated using a trypan blue assay, and a high production of reactive oxygen species was observed.

1. Introduction

Different shapes of nanomaterials have been utilized for killing cancerous cells over the last few years. Due to their high surface to volume ratio, nanomaterials possess striking characteristics. The applicability of nanomaterials depending on their shape as well as development is still under extensive study. For several decades, copper has been utilized as an antibacterial agent in either the form of ions or nanoparticles. The toxicity from various forms of copper nanoparticles is one of the major research topics. Usually, titanium dioxide, zinc oxide, and silver oxide nanoparticles exhibit a toxic response by oxidative stress,[1,2] dissolution-based toxicity,[3] and the Trojan horse mechanism.[4]

The physiochemical properties, stability, and dissolution of the different shapes of copper oxide nanoparticles exhibit a variety of responses in biological fluids.[1] Cuprous oxide nanoparticles selectively induce the apoptosis of tumor cells.[5] Not only the chemical nature but also the morphology may determine the toxic effects of the nanoparticles.[6,7] The antibacterial capacity based on the crystallography facet of Cu_2O has been studied.[8–10] The studies mentioned ROS-mediated oxidative stress and lipid peroxidation.[11–14] The different shapes of cuprous oxide nanocrystals play an important role due to their different properties like facet dependent catalytic, photocatalytic, electrical, and molecular adsorption.[15–20]

Cu_2O has been an area of high attention/interest for research due to its electronic structure.[21] It is a p-type metal oxide semiconductor[22] with a band gap of 2.0 eV. It is a promising material for applications in solar energy conversion, photocatalysis, biosensors, and the decomposition of O_2 and H_2 under visible light irradiation.[23,24] Recently, cuprous oxide nanocrystals have been synthesized *via* green methods.[25] The application of cuprous oxide nanocrystals as photocatalysts for hydrogen generation from a water/methanol mixture under UV/Vis irradiation has been reported. Nanocrystals possess superior catalytic properties over their bulk forms due to their large specific surface area and the short pathways for electron and hole transport.[26]

It is a well proven concept that on exposure to ultraviolet (UV-vis) light, the separation of electrons and holes on materials leads to the formation of reactive oxygen species, such as hydrogen peroxide, hydroxyl radical, and superoxide radicals.[27] These oxygen species are highly reactive with cell membranes and the cytoplasmic organelles, with the damaged areas depending on the particle's location upon excitation. Such oxidative reactions affect the cell rigidity and chemical arrangement of the surface structures, leading to cell toxicity.[28,29]

We proposed multi-faceted cuprous oxide nanocrystals for killing cancer cells *via* photodynamic therapy. Cubic, hexagonal and octahedral shapes were observed and a green laser was

[a]*Department of Chemistry and Center for Nanoscience and Nanotechnology, National Sun Yat-Sen University, Kaohsiung, 70, Lien-Hai Road, Kaohsiung, 80424, Taiwan. E-mail: hwu@faculty.nsysu.edu.tw; Fax: +886-7-5253909; Tel: +886-7-5252000 ext. 3955*

[b]*School of Pharmacy, College of Pharmacy, Kaohsiung Medical University, Kaohsiung, 807, Taiwan*

[c]*Institute of Medical Science and Technology, National Sun Yat-Sen University, 80424, Taiwan*

[d]*Doctoral Degree Program in Marine Biotechnology, National Sun Yat-Sen University, Academia Sinica, Kaohsiung, 80424, Taiwan*

† Authors with equal contributions (first author and co-first authors).

applied to produce reactive oxygen species to perform a ROS assay. With this, we demonstrated that the octahedral Cu_2O nanocrystals have the best photodynamic performance among these three shapes. Multi-faceted zero-dimensional Cu_2O nanocrystals can act as electron sinks and enhance the visible light photodynamic activity of the nanomaterials. On comparing the properties among the same dimensional nanomaterials, these impressive results will be significant for further exposure in this field. Cancer treatment utilizing Cu_2O nanocrystals as the photodynamic activity is still at a primitive level and it is essential to focus on these materials so that the best nanocrystals can be unraveled for various medical purposes.

2. Experimental

2.1 Materials and methods

Anhydrous copper chloride ($CuCl_2$), sodium dodecyl sulfate (SDS), dihydrorhodamine and hydrochloric acid were purchased from Sigma-Aldrich (USA). Sodium hydroxide was obtained from Janssen Chimica (Belgium). Hydroxylamine hydrochloride was ($NH_2OH \cdot HCl$) obtained from Alfa Aesar (Great Britain). Ultrapure water was provided from a Milli-Q Plus water purification system (18.2 MΩ cm, Millipore, and Bedford, MA, USA) and was used for all the experiments.

2.2 Instrumental utility

The structure and morphology of the as-synthesized Cu_2O nanocrystals were characterized by X-ray diffraction (XRD; Phillip, The Netherlands) and transmission electron microscopy (TEM, Phillip CM200, and Switzerland). The Fourier-transform infrared (FT-IR) spectra of cuprous oxide nanocrystals were obtained on an FT-IR spectrometer (Spectrum 100, Perkin Elmer, USA). An energy-dispersive X-ray spectrometer (EDX) (JOEL 6700F, Japan) was used for the surface elemental detection of the Cu_2O nanocrystals. UV-vis spectroscopy (Thermo, Evolution 201, and the USA) was used to study the spectral properties of the cuprous oxide nanocrystals.

2.3 Cell culture and treatment

HeLa cells were cultured in Dulbecco's modified eagle's medium (Sigma, St. Louis, Missouri, USA) with 10% fetal bovine serum (Gibco, Grand Island, New York, USA), 1% non-essential amino acids (Biosource, Camarillo, California, USA), 1% penicillin/streptomycin (Sigma, St. Louis, Missouri, USA), 1% sodium pyruvate (Sigma, St. Louis, Missouri, USA), and 1.5 g L^{-1} sodium bicarbonate (Sigma, St. Louis, Missouri, USA) in 5% CO_2 at 37 °C. The cells were trypsinized and seeded in tissue culture plates at an initial cell density of $\sim 10^5$ cells per well.

A cytotoxicity study was performed using a trypan blue staining assay.[30] HeLa cells were trypsinized and re-suspended in the culture medium. The cells were seeded in a tissue culture plate with 0.5 mL full of medium and kept overnight at 37 °C under 5% CO_2 atmosphere. Different concentrations of the cubic, hexagonal and octahedral Cu_2O nanocrystals suspensions were loaded to each well. Green laser ($\lambda = 532$ nm) was used for irradiation for a certain period of time. Subsequently, 0.4% trypan blue was added to each well, and after 5 min, the stained cells were counted to determine the cell viability. Unstained cells were counted as living cells and the blue stained cells were counted as dead cells.

The cell viability was measured using a 3-(4,5-dimethylthiazol-2-yl)-2,5-biphenyl tetrazolium bromide (MTT) assay. HeLa cells were seeded in a 96-well culture plate at a density of 2×10^4 cells per well and incubated at 37 °C. After overnight growth, the cells were treated with various concentrations (1–5 μg mL^{-1}) of the cubic, hexagonal and octahedral cuprous oxide nanocrystals and incubated for 24 h. Green laser irradiation ($\lambda = 532$ nm) was used for a certain period of time. Later, MTT was added to the cells, which were cultured for another 3 h and further analyzed at 570 nm.

2.4 Synthesis of different shapes of cuprous oxide nanocrystals (Cu_2O)

The synthetic protocol used to prepare the Cu_2O nanocrystals followed a literature procedure with slight modification.[24] Vials were labeled as (a), (b), and (c) containing 9.0, 8.5, and 7.0 mL of DI water, respectively. The sample vials were placed in a water bath at 33–34 °C. 0.5 mL of a 0.1 M $CuCl_2$ solution and 0.087 g of SDS powder were added to each vial with vigorous stirring. Moreover, 0.2 mL of a 1.0 M NaOH solution was added. The resulting solution immediately turned blue. After that, 0.4, 0.8 and 2.4 mL aliquots of a 0.1 M of $NH_2OH \cdot HCl$ solution were quickly injected into the vials (a, b, and c, respectively). Finally, all the contents in the vials were further diluted to 10 mL with DI water and continually stirred for 30 s. The solutions were kept in a water bath for 1 h for nanocrystal growth. After completion of the nanocrystal growth, the solutions were centrifuged at 5000 rpm for 5 min. The clear supernatant was removed, and the precipitate was washed thoroughly with an equal ratio of water and ethanol to remove the unreacted chemicals and SDS surfactants. The precipitate was centrifuged and washed again using the water/ethanol mixture to remove unreacted sodium dodecyl sulfate surfactant. Finally, the resulting solid was washed with only ethanol and stored as a suspension in ethanol.

2.5 ROS production and photodynamic studies

The generation of reactive oxygen species (ROS) was measured using dihydrorhodamine (DHR) dye. The dye (25 μM) was added to different concentrations of the Cu_2O nanocrystals and HeLa cells $\sim 1 \times 10^5$ cells per mL and irradiated with a green laser ($\lambda =$ 532 nm). Control cells were irradiated with laser in the absence of the nanocrystals. The fluorescence intensity of the dye was measured by excitation at 450 nm and observed at 530 nm. Eqn (1) was used for calculation, where the fluorescence intensities (F) are denoted as follows: F_{test} represents a solution containing the different nanoparticles and DHR dye, F_{blank} represents cuprous oxide in nanopure water, and $F_{control}$ represents the cuprous oxide nanoparticles in H_2O_2 solution with the DHR dye.

$$(F_{test} - F_{blank})/(F_{control} - F_{blank}) \times 100 \quad (1)$$

3. Results and discussion

3.1 Characterization of nanocrystals

A schematic of the synthesis of the different shapes of cuprous oxide nanocrystals (Fig. 1a) and their characterization evaluated by TEM, FTIR, XRD, and EDX, along with ROS production upon green laser irradiation are provided in Fig. 1b. Fig. 2 shows the TEM images and the corresponding electron diffraction patterns of the three nanocrystals. The pH values of all the three preparation solutions were decreased from basic to acidic (cubic = pH 10.78, hexagonal pH = 10.49; octahedral pH = 10.2), which is the key factor in determining the shape of the nanocrystals. As the pH decreases, the shape was modified from cubic, hexagonal and then to octahedral. The TEM images confirm the morphology with the results of the SEM images reported in the literature.[9] The average size of the nanocrystals was around 150–200 nm with surface orientation. As per earlier reports, the cubic, hexagonal and octahedral nanocrystals have increased in facets or surfaces, which are shown in the TEM images. In addition, the TEM images in Fig. 2 revealed that the single nanocrystals for each shape displayed a similar shape to those observed in groups.

The crystal structures of the Cu_2O nanocrystals were analyzed using XRD. Fig. 3a shows that the XRD patterns for all three nanocrystals look very similar in terms of their peak patterns. The XRD patterns show the expected (110), (111), (200), (220), (311), and (222) reflection peaks of Cu_2O and confirm that these nanocrystals have a cubic crystal structure of Cu_2O. The ratios of the intensity of the (200) peak to that of the (111) peak are continuously lowered from truncated cubic to the octahedral nanocrystals because of the decreasing (100) facets.

In addition, we confirmed the content of the nanocrystals. The elements of copper and oxygen were revealed in Fig. 3b. All these results showed that the nanocrystals have unique morphological shapes, with confirmed elements.

The optical properties of the cubic, hexagonal, and octahedral nanocrystals were determined by UV-vis absorbance spectroscopy, as shown in Fig. 4a. The nanocrystals display a full absorption band from 400 nm to 600 nm. The octahedral Cu_2O was observed to have a higher absorbance than those of the hexagonal and cubic samples. Cubic nanocrystals have a very low absorbance in the visible light region. The different absorption behavior of the cubic-, hexagonal-, and octahedral-shaped Cu_2O crystals may be related to the different atomic arrangement of their exposed surfaces. These nanocrystals showed a blue shift from the cubic to the octahedral shape.

Fig. 4b presents the FTIR spectra of the three shapes of Cu_2O nanocrystals. The IR spectrum of the as-synthesized cuprous oxide nanoparticles contains a band at 631 cm^{-1}, which was attributed to the Cu–O lattice vibrations. The band at 3270–3450 cm^{-1} arises from the –OH stretching vibrations of the surface-adsorbed water molecules. The absence of a stretching frequency for C–H bonds, which should appear in the range of 2850–2960 cm^{-1}, confirms that the crystal surface was free of any adsorbed surfactant.[6]

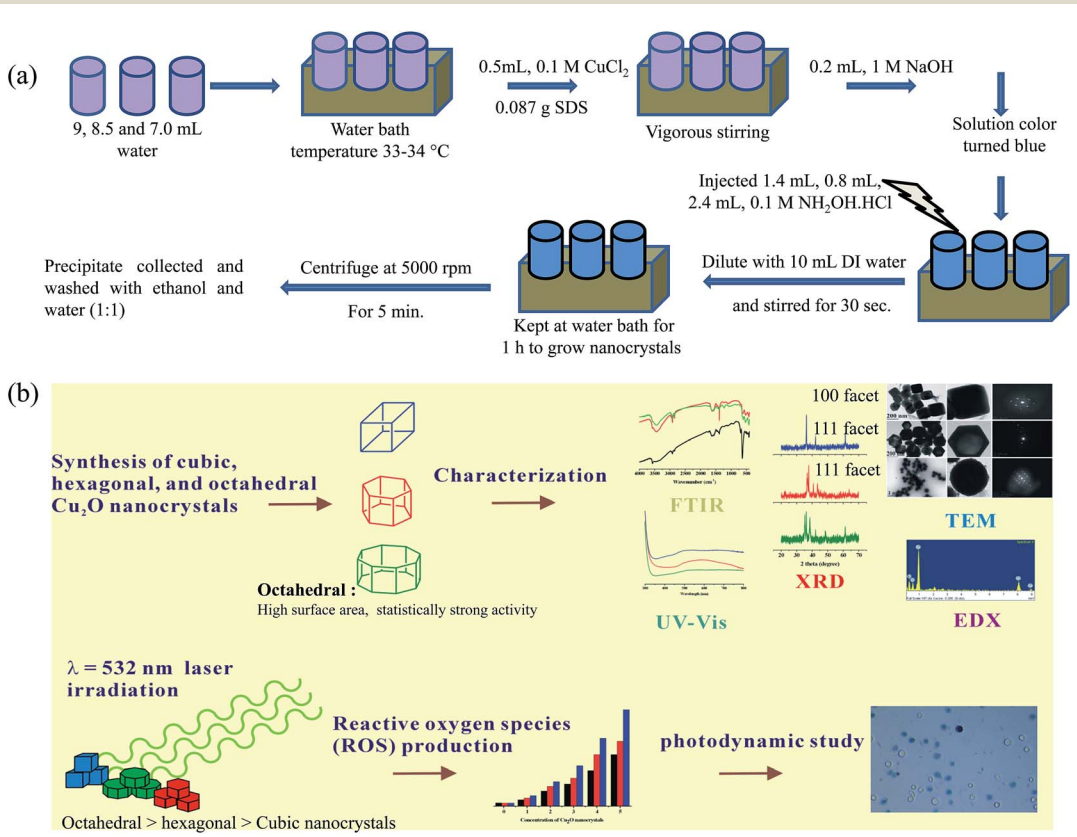

Fig. 1 (a) A schematic of the experimental procedures used to prepare different shapes of cuprous oxide nanocrystals (Cu_2O) and (b) their application in photodynamic activity using green laser irradiation.

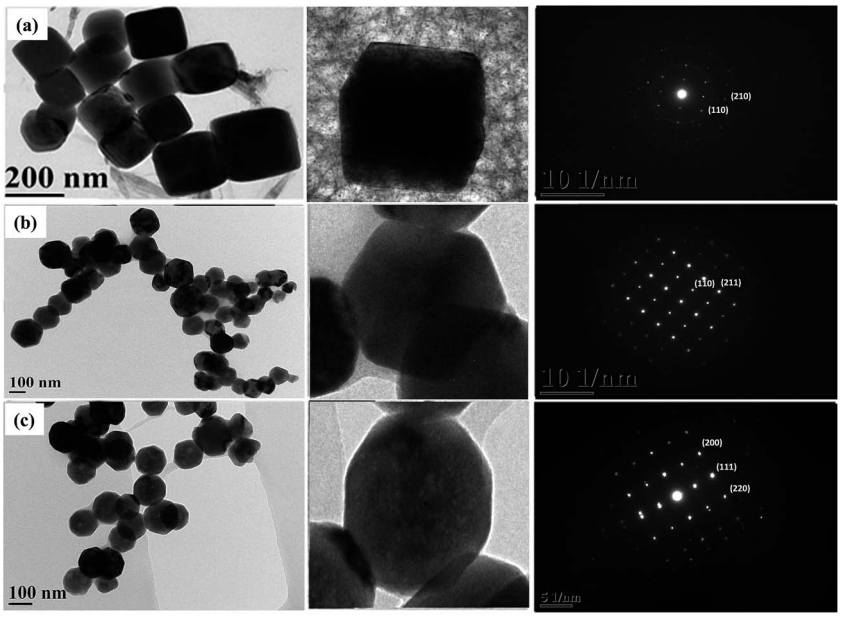

Fig. 2 TEM images with their respective SAED images of (a) cubic, (b) hexagonal and (c) octahedral cuprous oxide nanocrystals.

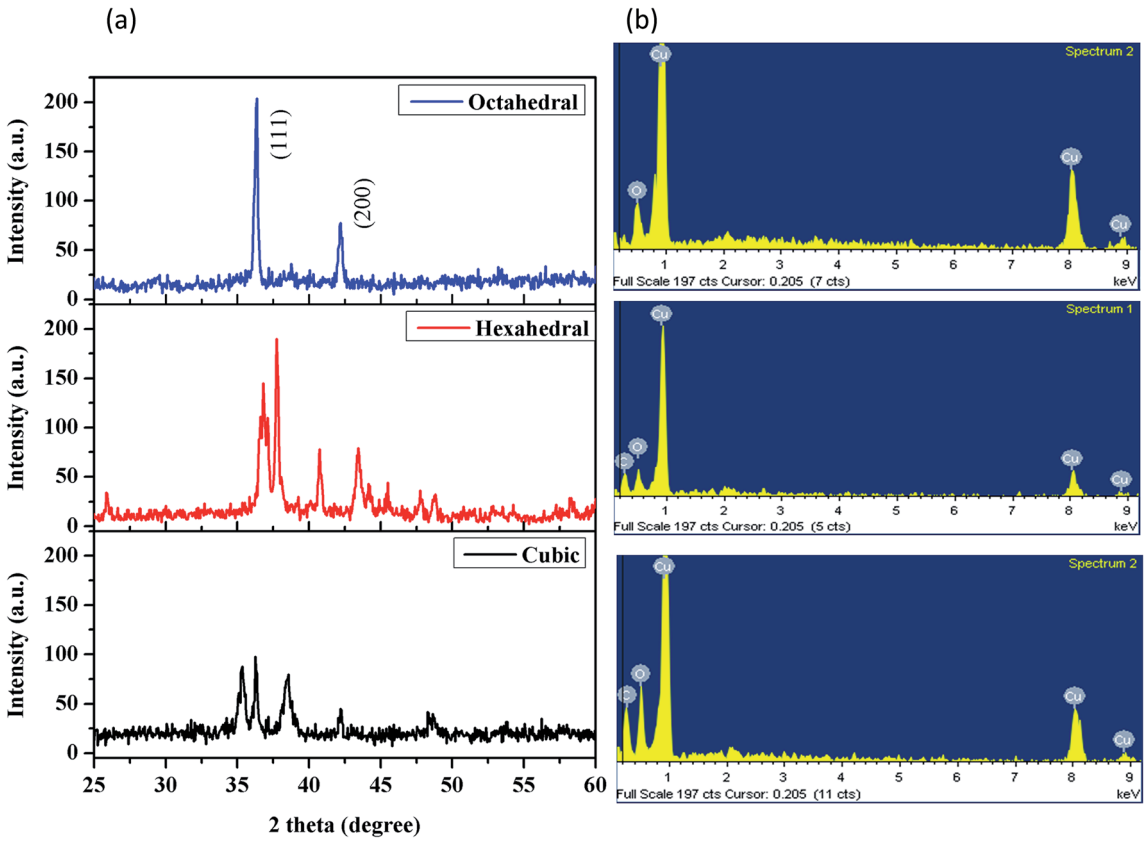

Fig. 3 Characterization of cubic, hexagonal and octahedral cuprous oxide nanocrystals: (a) XRD and (b) EDX spectra.

3.2 Shape-dependent ROS production by nanoparticles

Fig. 5 shows the production of ROS by different shaped Cu_2O nanocrystals irradiated by a green laser with dihydrorhodamine (DHR) dye. The ROS generation in the cubic, hexagonal, and octahedral shaped Cu_2O nanocrystals was comparatively studied. The difference in activity towards killing the cells was related to the specific surface area and the atomic arrangements of the exposed crystallographic facets. The octahedral sample

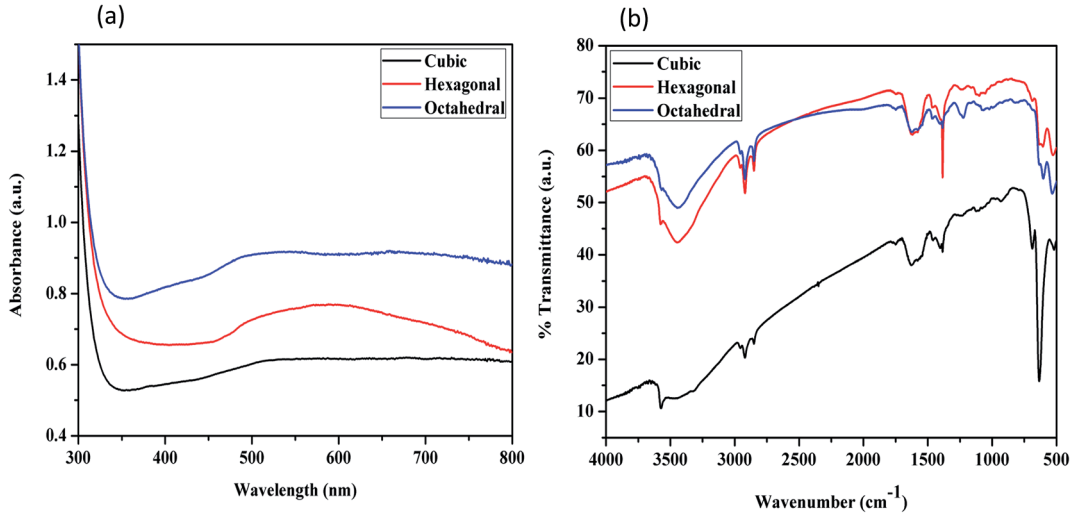

Fig. 4 Characterization of cubic, hexagonal and octahedral cuprous oxide nanocrystals: (a) UV-vis spectra; (b) FTIR spectra.

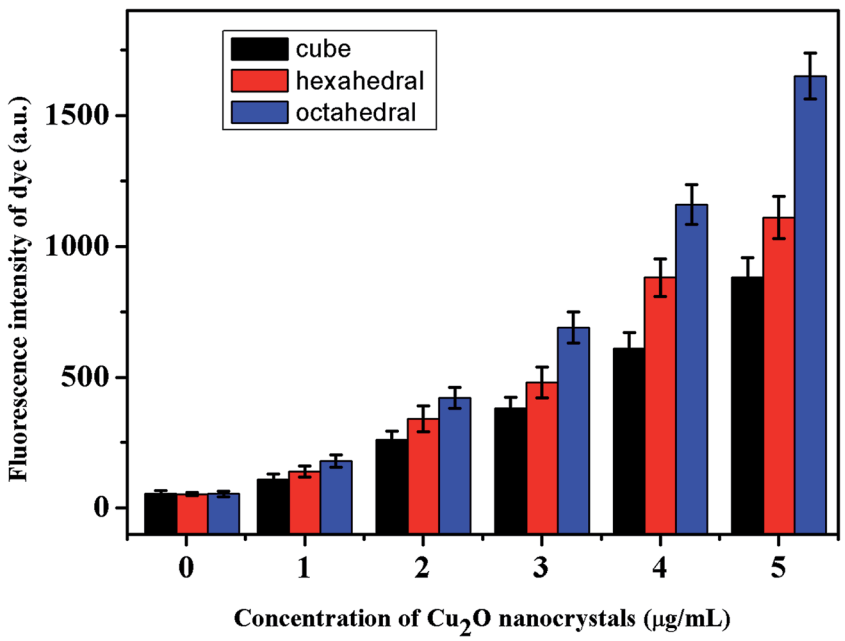

Fig. 5 ROS generation by the cubic-, hexagonal- and octahedral shaped cuprous oxide (1–5 μg mL^{-1}) after being treated with green laser irradiation.

has a larger specific surface area, and its particle arrangement make its surface energy higher than those of the hexagonal and cubic samples. Usually, the electron transfer needed for the formation of ROS has negligible interference from rhodamine and can be disregarded. Moreover, its low concentration does not contribute to the background ROS production. Due to the high surface area of the octahedral Cu_2O nanocrystals, they are more prone to have a statistically stronger activity than the hexagonal and cubic nanocrystals. The copper terminated structure will be relatively unstable due to the active interaction with the hydroxyl groups, generating more ROS. The order of ROS induced cells death was found to be octahedral Cu_2O > hexagonal Cu_2O > cubic Cu_2O.

3.3 Cu_2O nanocrystals laser induced cytotoxicity in HeLa cells

The visible light-induced cytotoxicity of the cuprous oxide nanocrystals was evaluated in the present study. After 2 h of incubation with the cuprous oxide nanocrystals, followed by green laser irradiation, the phototoxicity of cuprous oxide was tested using the trypan blue test. Furthermore, an experiment was performed on the viability of cancer cells using the trypan blue test. This was based on the principle that living cells possess intact cell membranes that exclude certain dyes, such as trypan blue. A viable cell holds a clear cytoplasm, whereas a non-viable cell can be colored, which is confirmed by blue cytoplasm.

Fig. 6 shows the cell viability of HeLa cells treated with the nanocrystals and irradiated with a green laser. Cancer cells were first treated with cubic, hexagonal and octahedral cuprous oxide nanocrystals, and their cell cytotoxicity was observed, as shown in Fig. 6c–h. In comparison to the treated cancer cells, the control group of untreated cancer cells showed a high viability of cells (Fig. 6a and b). From the ROS results generated from the irradiation of the nanocrystals by a green laser, additional

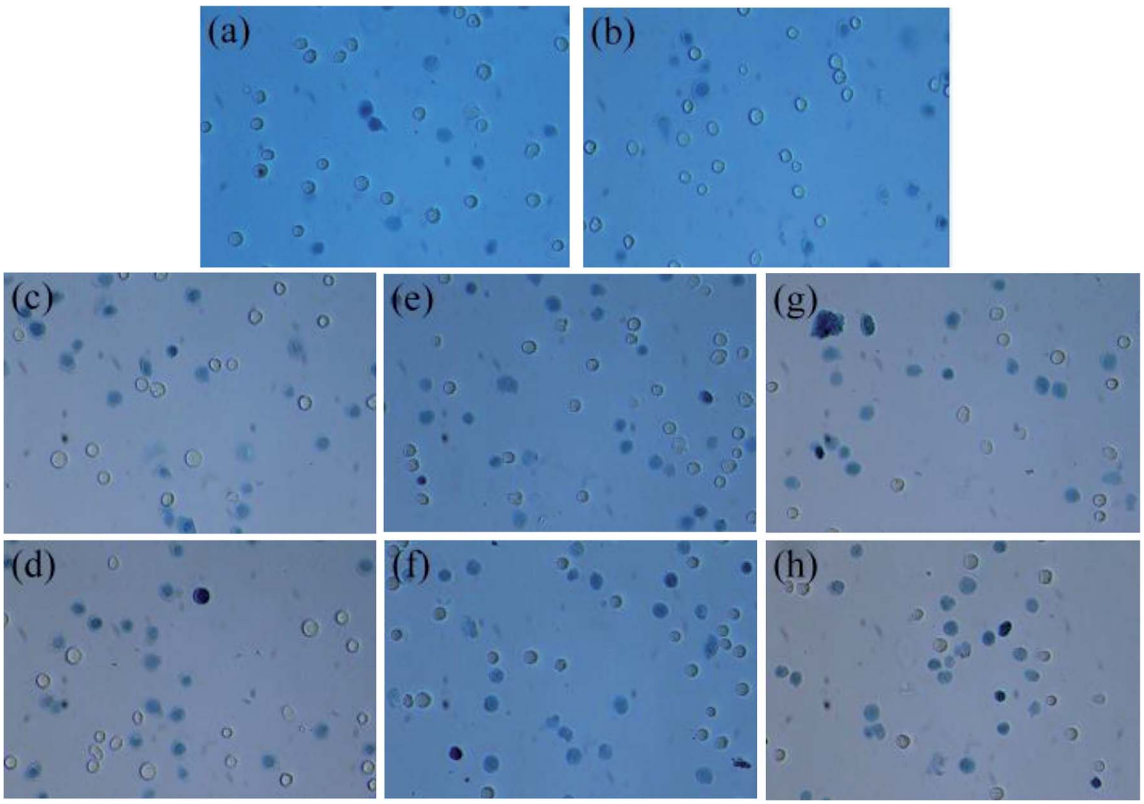

Fig. 6 A tryphan blue cytotoxicity assay for Cu_2O-treated cancer cells. Fluorescent microscope images of HeLa cells (a and b) incubated with cubic-, hexagonal- and octahedral shaped cuprous oxide nanocrystals (1–5 μg mL^{-1}): (c, e, g) and (d, f, h) indicate the lowest and highest concentrations of the individual cuprous oxide nanocrystals.

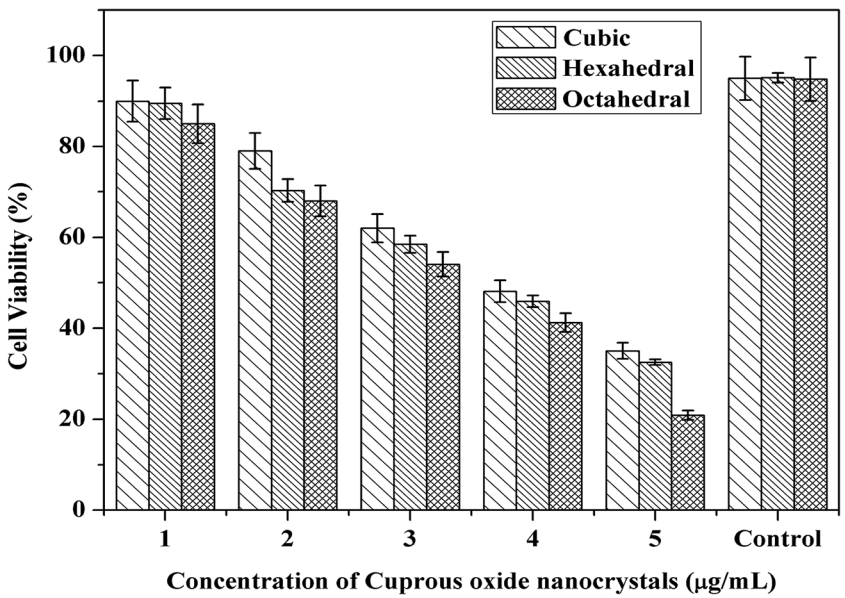

Fig. 7 An MTT assay representing HeLa cells treated with different concentrations of the cuprous oxide nanocrystals (1–5 μg mL^{-1}).

reliable evidence for the cytotoxicity of these nanocrystals can be provided. The concentration dependence of the cytotoxicity of the nanocrystals can be relatively observed by comparing the data in Fig. 6c, e, and g, where the cells were treated with lower concentrations of cubic, hexagonal and octahedral cuprous oxide nanocrystals, with the data in Fig. 6d, f and h, where the cells were applied with a higher concentration of the nanocrystals. The octahedral shape of cuprous oxide showed very potent phototoxicity upon laser irradiation, and the number of cells killed was the highest when compared to the live cells. The results indicate that the cell viability correspondingly decreased with increasing concentration of cuprous oxide nanocrystals. The viability of the cells that were pretreated with cuprous oxide nanocrystals at 1–5 μg mL^{-1}, followed by solid-state green laser (maximum output power 200 mW, at 532 nm) irradiation was decreased continuously compared to the that of the control group cells. This confirms that the photodynamic activity of cuprous oxide nanocrystals results from their ability to generate ROS when photo-excited. Cell death was not observed when the non-treated cell cultures were irradiated with a green laser under the above-described conditions. On extending the trypan blue experiment, an MTT assay was performed to determine the photodynamic activity of the cuprous oxide nanocrystals at different concentrations after irradiation with a green laser on the cancer cells (Fig. 7). It was clearly observed that increasing the concentration of the cuprous oxide nanocrystals results in the death of ~20% of the cancer cells. This also indicates that among the cubic, hexagonal and octahedral samples, octahedral Cu_2O shows a higher killing capacity compared to the other shapes. The photodynamic activity successfully established significant cancer cell death after green laser irradiation.

The significant difference between the reducibility of the octahedral, hexagonal and cubic Cu_2O nanocrystals should arise from their different surface structures, *i.e.*, different shapes. The reduction of an oxide always initiates from the surface. The cubic shaped crystal growth was observed at the {100} facet, while in the hexagonal or octahedral samples, the crystal growth was dominant at the {111} facets. The (111) facets are more active than the (100) facets due to the dangling bonds of the (111) surfaces, while no dangling bonds but saturated chemical bonds exist in the (100) facets. Therefore, the octahedral shaped nanocrystals exhibit a higher adsorption and photo-related activity than the hexagonal- and cubic-shaped nanocrystals. The octahedral and cubic Cu_2O nanocrystals expose the (111) and (100) crystal planes, respectively. In this experiment a type I-PDT was observed for cancer using the different shapes of cuprous oxide nanocrystals. The interpreted mechanism of radical ion formation in the Cu_2O suspension may occur as follows:

$$Cu_2O + h\nu \rightarrow e^- + h^+$$

$$OH^- + h^+ \rightarrow OH^{\cdot}$$

The hydroxyl radicals are generated *via* oxidation in the valence band, while in the conductance band an electron is donated to oxygen, thereby generating the superoxide radical anion.

4. Conclusions

Cu_2O nanocrystals with cubic, hexagonal, and octahedral morphology have been investigated to show a potential in photodynamic therapy for cancer treatment. The different crystalline structures of the nanocrystals enabled an investigation of their facet-dependent photodynamic therapy. The octahedral Cu_2O nanocrystals possess greater photodynamic activity compared to the cubic and hexagonal samples. Cancer cells can be eradicated by the generated reactive oxygen species *via* the irradiation of cuprous oxide nanocrystals using a green laser.

Acknowledgements

The authors acknowledge the financial support from the Ministry of Science and Technology (MOST) of Taiwan.

References

1 S. K. Misra, S. Nuseibeh, A. Dybowska, D. Berhanu, T. D. Tetley and E. Valsami-Jones, *Nanotoxicology*, 2014, **8**, 422–432.
2 Y. Li, W. Zhang, J. Niu and Y. Chen, *ACS Nano*, 2012, **6**, 5164–5173.
3 N. M. Franklin, N. J. Rogers, S. C. Apte, G. E. Batley, G. E. Gadd and P. S. Casey, *Environ. Sci. Technol.*, 2007, **41**, 8484–8490.
4 E.-J. Park, J. Yi, Y. Kim, K. Choi and K. Park, *Toxicol. in Vitro*, 2010, **24**, 872–878.
5 Y. Wang, X.-Y. Zi, J. Su, H.-X. Zhang, X.-R. Zhang, H.-Y. Zhu, J.-X. Li, M. Yin, F. Yang and Y.-P. Hu, *Int. J. Nanomed.*, 2012, **7**, 2641.
6 K. Chanda, S. Rej and M. H. Huang, *Nanoscale*, 2013, **5**, 12494–12501.
7 C. Saison, F. Perreault, J.-C. Daigle, C. Fortin, J. Claverie, M. Morin and R. Popovic, *Aquat. Toxicol.*, 2010, **96**, 109–114.
8 J. Ren, W. Wang, S. Sun, L. Zhang, L. Wang and J. Chang, *Ind. Eng. Chem. Res.*, 2011, **50**, 10366–10369.
9 C.-H. Kuo and M. H. Huang, *J. Phys. Chem. C*, 2008, **112**, 18355–18360.
10 Y.-W. Baek and Y.-J. An, *Sci. Total Environ.*, 2011, **409**, 1603–1608.
11 C. Gunawan, W. Y. Teoh, C. P. Marquis and R. Amal, *ACS Nano*, 2011, **5**, 7214–7225.
12 K. Giannousi, K. Lafazanis, J. Arvanitidis, A. Pantazaki and C. Dendrinou-Samara, *J. Inorg. Biochem.*, 2014, **133**, 24–32.
13 B. Fahmy and S. A. Cormier, *Toxicol. In Vitro*, 2009, **23**, 1365–1371.
14 M. Shi, H. S. Kwon, Z. Peng, A. Elder and H. Yang, *ACS Nano*, 2012, **6**, 2157–2164.
15 N. Serpone and E. Pelizzetti, *Photocatalysis: Fundamentals and Applications*, Wiley, New York, 1989.
16 N.-P. Huang, X. Min-Hua, C.-W. Yuan and Y. Rui-Rong, *J. Photochem. Photobiol., A*, 1997, **108**, 229–233.
17 A.-P. Zhang and Y.-P. Sun, *World J. Gastroenterol.*, 2004, **10**, 3191–3193.
18 S. Wang, R. Gao, F. Zhou and M. Selke, *J. Mater. Chem.*, 2004, **14**, 487–493.

19 C. Hou, H. Quan, Y. Duan, Q. Zhang, H. Wang and Y. Li, *Nanoscale*, 2013, **5**, 1227–1232.
20 B. Z. Ristic, M. M. Milenkovic, I. R. Dakic, B. M. Todorovic-Markovic, M. S. Milosavljevic, M. D. Budimir, V. G. Paunovic, M. D. Dramicanin, Z. M. Markovic and V. S. Trajkovic, *Biomaterials*, 2014, **35**, 4428–4435.
21 S. Lee, C.-W. Liang and L. W. Martin, *ACS Nano*, 2011, **5**, 3736–3743.
22 M. Yin, C.-K. Wu, Y. Lou, C. Burda, J. T. Koberstein, Y. Zhu and S. O'Brien, *J. Am. Chem. Soc.*, 2005, **127**, 9506–9511.
23 A. Singhal, M. R. Pai, R. Rao, K. T. Pillai, I. Lieberwirth and A. K. Tyagi, *Eur. J. Inorg. Chem.*, 2013, **2013**, 2640–2651.
24 W.-C. Huang, L.-M. Lyu, Y.-C. Yang and M. H. Huang, *J. Am. Chem. Soc.*, 2011, **134**, 1261–1267.
25 H. Zheng, Q. Li, C. Yang, H. Lin, M. Nie, L. Qin and Y. Li, *RSC Adv.*, 2015, **5**, 59349–59353.
26 Z. Yu, C. M. Wang, M. H. Engelhard, P. Nachimuthu, D. E. McCready, I. Lyubinetsky and S. Thevuthasan, *Nanotechnology*, 2007, **18**, 115601.
27 Z. Hu, Y. Huang, S. Sun, W. Guan, Y. Yao, P. Tang and C. Li, *Carbon*, 2012, **50**, 994–1004.
28 T. Mahalingam, J. Chitra, G. Ravi, J. Chu and P. Sebastian, *Surf. Coat. Technol.*, 2003, **168**, 111–114.
29 W. Fan, X. Wang, M. Cui, D. Zhang, Y. Zhang, T. Yu and L. Guo, *Environ. Sci. Technol.*, 2012, **46**, 10255–10262.
30 H. Lin, T. Y. Lin and J. L. Juang, *Cell Death Differ.*, 2007, **14**, 607–615.